Jurnal Teknologi

Full paper

Development of a New Method of Sensitivity Matrix for Image Reconstruction in Electric Charge Tomography System Using Finite Element Method

Iliya Tizhe Thuku[a], Mohd Fua'ad Rahmat[b*]

[a]*Department of Electrical and Electronics Engineering, School of Engineering and Engineering Technology, Modibbo Adama University of Technology P.M.B 2076 Yola Adamawa State Nigeria*
[b]*Control and Mechatronics Engineering Department, Faculty of Electrical Engineering, Universiti Teknologi Malaysia, 81310 UTM Johor Bahru, Johor, Malaysia*

*Corresponding author: fuaad@fke.utm.my

Article history

Received :5 February 2014
Received in revised form :
7 April 2014
Accepted :20 May 2014

Graphical abstract

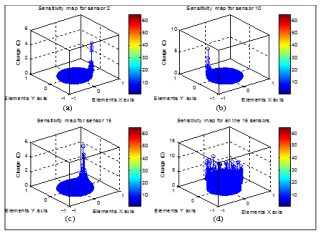

Abstract

In this paper, a new method of sensitivity matrix generation is presented for application in electric charge tomography system. The sensitivity matrix is the most important parameter in solid particles concentration profile computation in electric charge tomography system. The analytical method of developing the sensitivity matrix that have been developed and used in electric charge tomography is characterised by some uncertainties that give poor tomography images of flowing solid particles. The new proposed method involved subdivision of the pipeline cross-section into many subdivisions called the computational mesh. The subdivision is made by the application of the Finite Element Method (FEM). On each of the electrodynamic sensor installed to detect the electric charges carried by the moving solid particles; the effect of the particles' electric charges enclosed in each of the computational mesh is modelled into a system equation. The system equation is used to compute the effect of the charges in the form of a matrix system of size [M×N] called the sensitivity matrix. The sensitivity matrix is applied for the reconstruction of the tomography image, using the Linear Back Projection (LBP) method. The reconstructed images represented the solid particles distribution through the pipeline. This assertion is due the consistencies between the simulation and real images with respect to the simulated images and the captured real data.

Keywords: Sensitivity matrix; electric charge tomography; condition number; linear back projection; concentration profile

1.0 INTRODUCTION

There are a lot of interests these days in knowing the exact behaviour of internal flow in process equipment. The enthusiasm is due to the need to increase the production efficiencies of the industries that uses conveying equipment such as pipelines, in their production system in order to meet up with; legislative and environmental requirements, product's qualities and demand, as well as minimizes operational hazards [1, 2]. Tomography originates from two Greek words *'tomo'* and *'graph'*; meaning; slicing or cutting or a section and picture respectively [3]. It is also defined as a technique for displaying a representation of cross sections of object [4]. The industrial tomographic imaging is a process tomography that provides real-time cross-sectional images of the distribution of materials in a process and has been developed as reliable tools for imaging various industrial processes over the last decades[5, 6]. In process tomography image reconstruction, sensitivity matrix which is the matrix of the measure of the ability of each sensor around the sensing zone, to detect properties of interest such as; permittivity, conductivity, electrical charges, etc.; in the sensing zone is the most important parameter. The sensitivity matrix otherwise called the image pixel, in tomography imaging, is the building blocks by which, tomographic image is being reconstructed. In electric charge tomography system, electric charge is the parameter of interest. In the electric charge tomography image reconstruction system, the method normally used for the generation of the sensitivity matrix is the one proposed and used in [3, 7-9]. In the proposed method of the sensitivity matrix, set of square boxes of 9×9, 11×11, 16×16 were created through which a circle of cross-sectional radius equal to the conveying pipe is drawn as shown in Figure 1. The 16 electrodynamic sensors were equally spaced around the circumference of the circle with location coordinates of the sensors as (x, y) shown in the (b) part of the Figure 1.

It was based on the Figure 1 that; the effect of the electrostatic charges carried by the particles flowing through the pipeline is quantified on the installed sensors. This method of generating sensitivity matrix is prone to the problems of; imprecise locations of the sensors and the coordinates of the

squares. Other source of the problem is that the pipe's cross-section did not completely cover the squares that formed the image pixels. These problems lead to the reconstruction of false images outside the pipe cross-section [10].

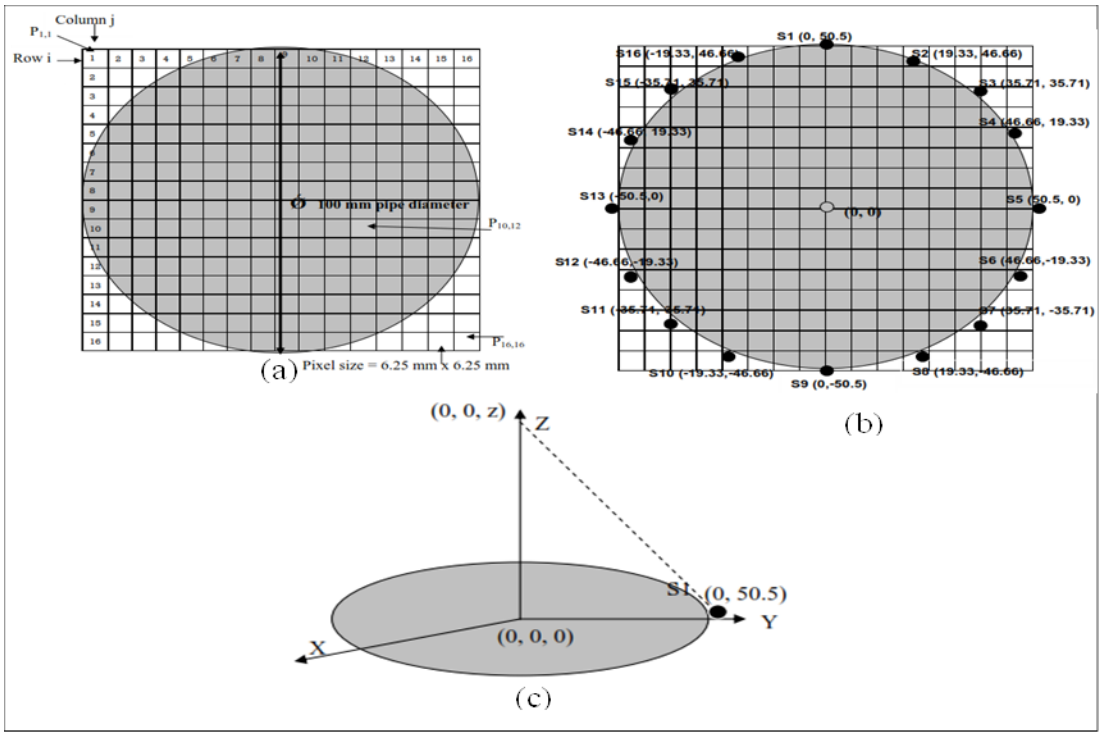

Figure 1 Sensitivity generation model [3]

To address this problem a new method of sensitivity generation for electric charge tomography image reconstruction method is proposed. In the proposed method, Finite Element Method (FEM) is used for subdividing the pipeline cross-section into many subdivisions called the finite element or computational mesh [11]. On each of the mesh elements, the effects of electrostatic charges on each of the 16 installed electrodynamic sensors were modeled into a system equation. The modeled system equation was used to generate the sensitivity matrix. For experimentation, the standard laboratory test rig for electric charge tomography system was used. LBP method was used to reconstruct 4 flow regimes tomography images of plastic beads particles that flow under gravity, through the experiment's pipeline of the test rig. To test the stability of the system and the accuracy of the image data; stability and error analyses were carried which gave good results. However, the proposed new method of the sensitivity matrix development, gave a good representation of the distribution of the flowing solid particles, through the pipeline cross-section. The method seems to be a good candidate for application in other electric charge tomography instrumentation systems; such as mass flow rate, velocity profile, particle position identification, particle sizing etc.

2.0 FORWARDMODELING

The forward modelling involved the development of the system equation, by which the sensitivity matrix is to be generated. The system equation is modelled in terms of the Cartesian coordinates of the domain mesh elements and the sensors installed at a test point around the periphery of the pipeline as shown in Figure 2. The Figure 2, shows electrodynamic sensors whose details are presented in [11] that are used in the research for the detection of the electrostatic charges carried by the moving solid particles. The configuration of the sensors in practical terms is shown in the Figure 2. In the Figure 2(a), the 16 electrodynamic sensors are installed at a test point, around the conveying pipeline, while the (b) part of the Figure 2 shows the spacing and numbering of the sensors.

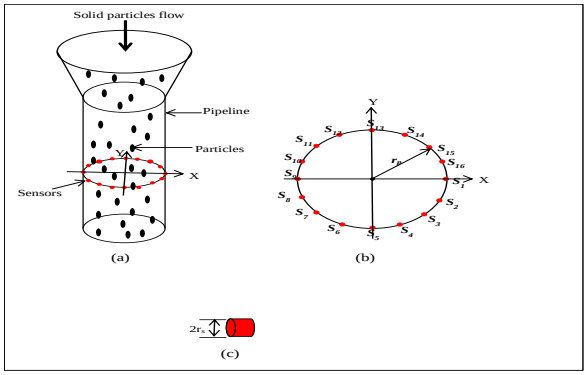

Figure 2 The electrodynamic sensor configuration (a) diagram of pipeline with sensors installed, (b) pipeline cross-section and (c) sensor pin electrode of radius r_s

The idea behind the use of the Cartesian coordinate is due to the fact that; the effect of electric field due to electric charge is a function of the distance between the source of the electric charge and the point at which the effect is to be computed. It was also found that; "*If two lines "P" and "Q" are drawn through two points "a" and "c" parallel to the axis "X" and "Y" respectively, in which, point 'a' is inside a circle and 'c' is*

at the circumference of the circle, the two lines 'P' and 'Q' meet at point "b" inside the circle to form a right angled triangle "abc" whose hypotenuse is the distance between the two points "a" and "c" i.e., line a-c"; as shown in the Figure 3. By the use of the Cartesian coordinates of the points 'a' and 'c', the opposite and adjacent lines of the right angled triangle 'abc' can be obtained; based on which the distance between the two points 'a' and 'c' is easily obtained by the application of Pythagoras theorem.

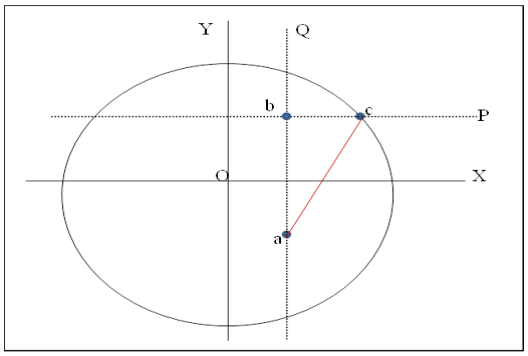

Figure 3 Mathematical modelling concept diagram

In modelling of the equations, it is assumed, that the particles move parallel to the pipe's Z-axis. Consider a 3-D section of a pipeline of radius r_p, with the pin electrode sensors of radius r_s installed around a test point of the pipeline circumference as shown in Figure 4. The 3-D pipe section of the Figure 4(a) shows the section of the pipeline cross-section at where the sensors are installed. The Figure 4 also shows an element being exaggerated on the plane of the cross-section and the surface area of the element is A_e,. The Figure 4(b) shows a typical mesh element with electric flux lines radiating from it; due to the enclosed electrostatic charges carried by the flowing solid particles. The Cartesian central coordinates of the mesh element *i* and sensor *n* are $e_i(x_i, y_i)$and $S_n(x_n, y_n)$. For the modelling, the triangle adc in the Figure 4(a) is on the Z plane while the triangle abc is on the X-Y plane. The detailed system Equation (1) derivation is in [1].

$$Q_{sn}(i) = -\frac{\pi r_s^3 \sigma}{4r_p\sqrt{(x_i-x_n)^2+(y_i-y_n)^2}\sqrt{(x_i-x_n)^2+(y_i-y_n)^2+r_s^2}} \quad (1)$$

Where

$Q_{sn}(i)$ = the charges induced in sensor *n* due to the charges enclosed in element *i* surface area

A_e = Surface area of element *i*

r_p= the pipeline cross-sectional radius

r_s= the sensor electrode radius

(x_i,y_i) and (x_n,y_n)= the Cartesian coordinates of the i^{th} mesh element and n^{th} sensor respectively.

Figure 3 is analogous to the x-y plane of the Figure 4 around the centres of the sensor electrodes, whereby, the triangles 'abc' in the both Figures are the same. It is imperative to note that; the point 'a' is the centre of each of the reference mesh element while point 'c' is the respective centre of the electrodynamic sensor electrode, installed at the circumference of the conveying pipeline cross-section.

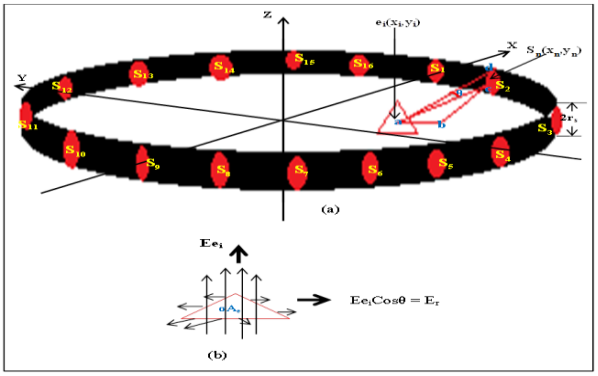

Figure 4 The system equation modelling diagram; (a) pipe strip cross-section and (b) domain element [11]

2.1 Generation of the Sensitivity Matrix

To generate the sensitivity matrix, the cross-section of the conveying pipeline is subdivided into finite elements and the process is called domain meshing. The meshing of the domain can be done in two ways, thus; auto meshing and structured meshing. In order to control and position the mesh (which is not feasible in auto-mesh), structured mesh generation is applied in this work. The structured meshing is favoured because of the difficulty in control the mesh size and position in auto-meshing, judged from the previous similar researches [12-14] in which, meshes were generated everywhere without specific points of applications. To mesh the pipeline cross-section at the specific experiment point, Matlab computer program was developed to structurally mesh the domain and also obtain the central coordinates of each of the mesh elements as well as the centre coordinates of the installed sensor electrodes. With the mesh parameters, the equation (1) was used to generate the sensitivity matrix applied in the tomography image reconstruction. However, the Matlab computer program was developed and ran to mesh the pipeline cross-section as shown in Figure 5. The Figure 5(a) is the domain, meshed into 1761 triangular element, with total nodes of 930, while (b) is the plot of the central Cartesian coordinates of the mesh elements.

The Figure 5 also shows the electrodynamic sensors, equally spaced around the periphery of the pipeline around at the test point. The developed program also computes the Cartesian coordinates of the installed sensors.

The Tables 1 and 2 presents the value of the x and y Cartesian coordinates of the centres of the elements and the sensor electrodes respectively, obtained from the result of the Matlab computer program. Note that; the cross-sectional radius 'r_p' of the pipeline used for the experimentation is 54 mm while the sensor electrode radius 'r_s' is 2.4 mm.

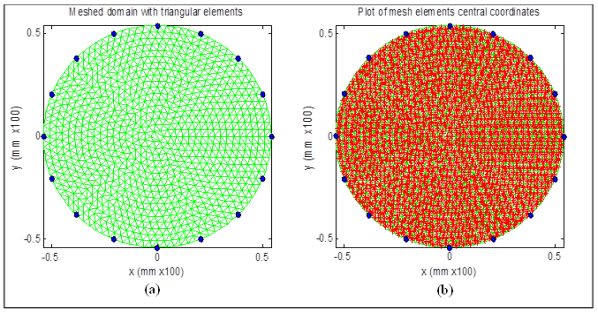

Figure 5 Plots of (a) meshed domain (b) domain elements' central coordinates

The Table 3 presented extract from the generated sensitivity matrix, which is to be used for the tomography image reconstruction also called the concentration profile of the flowing solid particles. To generate the data of Table 3, an assumed electric areal charge density 'σ' is made to be 1 Cm^{-2}.To test the viability of the generated sensitivity matrix, plots of the sensitivity characteristics of the sensors called "the sensitivity maps" are made for all the 16 sensors. The sensitivity maps for 4 of the 16 sensors are shown in Figure 6. The sensitivity maps display how each sensor view the distribution of the particles across the pipeline cross-section.

Table 1 Sensors central coordinates

Coord.	Sensor S_n and its central Cartesian coordinates															
	S_1	S_2	S_3	S_4	S_5	S_6	S_7	S_8	S_9	S_{10}	S_{11}	S_{12}	S_{13}	S_{14}	S_{15}	S_{16}
x_n	0.50	0.38	0.21	0.00	-0.21	-0.38	-0.50	-0.54	-0.50	-0.38	-0.21	0.00	0.21	0.38	0.50	0.54
y_n	-0.21	-0.38	-0.50	-0.54	-0.50	-0.38	-0.21	0.00	0.21	0.38	0.50	0.54	0.50	0.38	0.21	0.00

Table 2 Extract from elements centre coordinates

Coord.	Element e_i and its central Cartesian coordinates														
	e_1	e_2	e_3	e_4	e_5	e_6	e_7	e_8	e_9	e_{10}	e_{11}	e_{12}	e_{13}	--	e_{1761}
x_i	0.45	-0.03	-0.29	0.35	-0.25	-0.4	-0.29	-0.17	0.01	-0.4	0.11	-0.31	-0.18	--	0.41
y_i	-0.28	-0.11	-0.02	0.25	-0.7	0.04	0.02	0.31	-0.05	0.19	0.01	0.22	0.47	--	-0.33

Table 3 Extract from system's sensitivity matrix generated using the system equation

Element No.	Sensor's sensitivity value per element (i)															
	S_1	S_2	S_3	S_4	S_5	S_6	S_7	S_8	S_9	S_{10}	S_{11}	S_{12}	S_{13}	S_{14}	S_{15}	S_{16}
e_1	0.99	0.66	0.25	0.15	0.11	0.09	0.08	0.07	0.07	0.07	0.08	0.08	0.10	0.12	0.17	0.28
e_2	0.15	0.16	0.18	0.19	0.19	0.18	0.17	0.15	0.14	0.13	0.13	0.12	0.12	0.12	0.13	0.14
e_3	0.10	0.10	0.11	0.13	0.16	0.22	0.29	0.33	0.27	0.20	0.15	0.13	0.11	0.10	0.10	0.09
-	-	-	-	-	-	-	-	-	-	-	-	-	-	-	-	-
-	-	-	-	-	-	-	-	-	-	-	-	-	-	-	-	-
e_{1761}	0.54	1.47	0.31	0.18	0.12	0.10	0.08	0.08	0.07	0.07	0.07	0.08	0.09	0.11	0.15	0.23

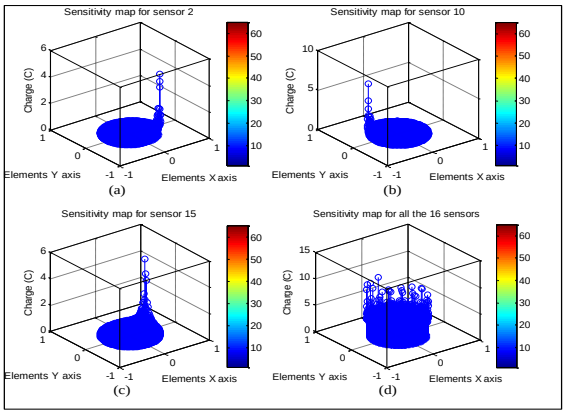

Figure 6 Sensitivity maps for randomly selected sensors 2, 10, 15 and all the 16 sensors combined

■3.0 THE IMAGE RECONSTRUCTION USING THE LINEAR BACK PROJECTION (LBP) METHOD

To experiment the sensitivity matrix for the image reconstruction in the electric charge tomography system, LBP method is applied. The LBP is an image reconstruction method in tomography by which the distributed charge q is related to the voltage sensed by installed sensors [15], as;

$$V = Sq \quad (2)$$

Where

S = the sensitivity matrix with a square dimension of the number of installed sensors

V = the average d.c voltage vector measured from the sensors outputs

q=the Charge distribution vector to be calculated.

Reconstruction of images using this method is an inverse problem to be solved using the Equation (3). The major problem associated with the method is the existence of inverse of matrix S [16] or else the general concept of inverse matrix is applied to equation (3) to get $q=S^{-1}V$ [17] known as back projection. In reality, *S* must be a symmetric matrix; as such, the general LBP equation can be formulated as;

$$qLBP = SV \quad (3)$$

Nevertheless, the sensitivity matrix obtained that is presented in Table 3, is a rectangular matrix, with dimension, [1761×16]; which can easily be made to square and invertible by the application of matrix transposition operation [18]. However, the transposition operation was carried out on the system matrix of the Table 3, and the result is shown in Table 4. The Table 4 is used for the tomography image reconstruction using the LBP method. For the validation of the developed sensitivity matrix used for the image reconstruction, simulation and real image reconstruction was carried out as presented in the subsections 3.1 and 3.2 respectively.

3.1 The Simulation Image Reconstruction using the LBP Method

The Figure 7 shows the baffling arrangements around the data capturing segment of the conveying pipeline for the experimentation of artificially created 4 different flow regimes. The flow regimes are ¼-flow, ½-flow, ¾-flow and Full-flow. The electrodynamic sensors are well placed and numbered as can be seen in the Figure 7. The recorded voltages V_i are the vectors to be used with the computed sensitivity matrix for the reconstruction of the real particles distribution across the pipe cross-section otherwise known as concentration profile or tomographic image of the flowing solid particles.

For the simulation of the image of ¼-flow regime, it is assumed that the flowing particles passes through only ¼ of the pipe cross-section, and that, only ¼ of the total sensors are active while the remaining are dormant. The same assumptions were made for ½-flow, ¾-flow and Full-flow regimes. The choice on which of the sensor is to be made high for the purpose of simulation, is based on experimental particles baffling arrangement of the Figure 7. However, Table 4 shows the sensors' simulation induced voltages during the four flow regimes, which is presented in bar charts in Figures 8(a)–(d).

The assumed induced voltages by the sensors were used with the transposed sensitivity matrix of Table 5, to reconstruct the simulation concentration profiles of the 4 different flow regimes. The simulation concentration profiles or tomography images for the 4 flow regimes are shown in Figure 9 in 2-D and 3-D. To reconstruct the tomography images, direct application of the LBP formula of Equation (3) was applied to generate the LBP image data for all the flow regimes as shown in Tables 6, 7, 8 and 9. Since the transposed sensitivity matrix S_t in Table 5 is invertible, the Equation (3) can be written as;

$$q_{LBP} = S_t^{inv.} V_s \quad (4)$$

Where

q_{LBP} = linearly projected charge distribution

$S_t^{inv.}$ = inverse of the transposed sensitivity matrix

V_s = the average d.c voltages measured by the installed electrodynamic sensors

However, the V_s are presented in the Table 4, that were taken to be experimentally induced average voltages from each of the sensors. For the ¼-flow regime, sensors 11 to 14 are active, while 1 to 10 and 15, 16 are dormant; for ½-flow, sensors 9 to 16 are active while 1 to 8 are dormant, for ¾-flow, sensors 1 to 10, 15 and 16 are active while sensors 11 to 14 are dormant and for Full-flow, all the sensors are active while none is dormant; all the assumptions are based on the sensor locations in the Figure 7.

Table 4 Assumed induced average d.c voltage by sensors for the simulation

Flow Regimes	Voltages (v_s) from sensors															
	S_1	S_2	S_3	S_4	S_5	S_6	S_7	S_8	S_9	S_{10}	S_{11}	S_{12}	S_{13}	S_{14}	S_{15}	S_{16}
¼-flow	0	0	0	0	0	0	0	0	0	0	1	1	1	1	0	0
½-flow	0	0	0	0	0	0	0	0	1	1	1	1	1	1	1	1
¾-flow	1	1	1	1	1	1	1	1	1	1	0	0	0	0	1	1
Full-flow	1	1	1	1	1	1	1	1	1	1	1	1	1	1	1	1

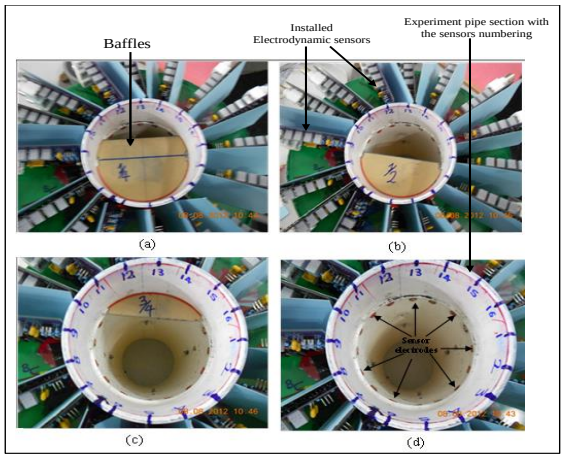

Figure 7 Particle flow control arrangement; (a) ¼-flow regime, (b) ½-flow regime, (c) ¾-flow regime and (d) Full–flow regime [11]

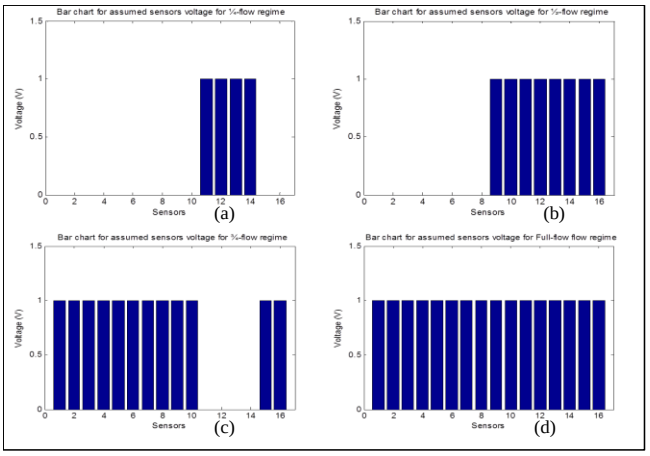

Figure 8 Bar charts of the assumed voltage used for the simulation for; (a) ¼-flow (b) ½-flow (c) ¾-flow and (d) full-flow

Table 5 The transposed system's sensitivity matrix generated from the system equation

Pixel No	Sensor's sensitivity value per pixel (i)															
	S_1	S_2	S_3	S_4	S_5	S_6	S_7	S_8	S_9	S_{10}	S_{11}	S_{12}	S_{13}	S_{14}	S_{15}	S_{16}
P_1	167.21	95.70	72.90	61.26	54.02	49.40	46.63	45.04	44.52	44.93	46.54	49.44	53.91	61.08	72.89	96.30
P_2	95.70	166.49	95.70	73.15	61.22	53.99	49.52	46.63	45.03	44.42	44.94	46.55	49.32	53.90	61.08	73.19
P_3	72.90	95.70	165.52	96.23	73.11	61.20	54.14	49.53	46.63	44.93	44.44	44.96	46.46	49.32	53.90	61.29
-	-	-	-	-	-	-	-	-	-	-	-	-	-	-	-	-
-	-	-	-	-	-	-	-	-	-	-	-	-	-	-	-	-
P_{16}	96.30	73.19	61.29	54.20	49.55	46.64	45.14	44.64	45.14	46.64	49.55	54.20	61.29	73.19	96.31	181.70

Table 6 Simulation image data for LBP in ¼ -flow regime

Pixel No	Charge magnitude in (C) per sensor due to electric charge in pixel (i)															
	S_1	S_2	S_3	S_4	S_5	S_6	S_7	S_8	S_9	S_{10}	S_{11}	S_{12}	S_{13}	S_{14}	S_{15}	S_{16}
P_1	0	0	0	0	0	0	0	0	0	0	-1.03×10^{-4}	-1.14×10^{-4}	-2.05×10^{-4}	-3.31×10^{-4}	0	0
P_2	0	0	0	0	0	0	0	0	0	0	-8.81×10^{-5}	-8.89×10^{-5}	-1.41×10^{-4}	-1.89×10^{-4}	0	0
P_3	0	0	0	0	0	0	0	0	0	0	-9.12×10^{-5}	-8.42×10^{-5}	-1.20×10^{-4}	-1.41×10^{-4}	0	0
- -	- -	- -	- -	- -	- -	- -	- -	- -	- -	- -	- -	- -	- -	- -	- -	- -
P_{16}	0	0	0	0	0	0	0	0	0	0	-1.04×10^{-4}	-1.29×10^{-4}	-2.71×10^{-4}	-5.70×10^{-4}	0	0

Table 7 Simulation image data for LBP in ½ -flow regime

Pixel No	Charge magnitude in (C) per sensor due to electric charge in pixel (i)															
	S_1	S_2	S_3	S_4	S_5	S_6	S_7	S_8	S_9	S_{10}	S_{11}	S_{12}	S_{13}	S_{14}	S_{15}	S_{16}
P_1	0	0	0	0	0	0	0	0	-7.63×10^{-5}	-9.92×10^{-5}	-1.03×10^{-4}	-1.14×10^{-4}	-2.05×10^{-4}	-3.31×10^{-4}	-7.97×10^{-4}	-3.25×10^{-3}
P_2	0	0	0	0	0	0	0	0	-7.88×10^{-5}	-9.36×10^{-5}	-8.81×10^{-5}	-8.89×10^{-5}	-1.41×10^{-4}	-1.89×10^{-4}	-3.31×10^{-4}	-5.70×10^{-4}
P_3	0	0	0	0	0	0	0	0	-9.88×10^{-5}	-1.07×10^{-4}	-9.12×10^{-5}	-8.42×10^{-5}	-1.20×10^{-4}	-1.41×10^{-4}	-2.05×10^{-4}	-2.72×10^{-4}
- -	- -	- -	- -	- -	- -	- -	- -	- -	- -	- -	- -	- -	- -	- -	- -	- -
P_{16}	0	0	0	0	0	0	0	0	-6.42×10^{-5}	-9.10×10^{-5}	-1.04×10^{-4}	-1.29×10^{-4}	-2.71×10^{-4}	-5.70×10^{-4}	-3.25×10^{-3}	9.81×10^{-3}

Table 8 Simulation image data for LBP in ¾ -flow regime

Pixel No	Charge magnitude in (C) per sensor due to electric charge in pixel (i)															
	S_1	S_2	S_3	S_4	S_5	S_6	S_7	S_8	S_9	S_{10}	S_{11}	S_{12}	S_{13}	S_{14}	S_{15}	S_{16}
P_1	1.12×10^{-2}	-3.77×10^{-3}	-6.93×10^{-4}	-2.56×10^{-4}	-1.78×10^{-4}	-1.39×10^{-4}	-8.91×10^{-5}	-8.20×10^{-5}	-7.63×10^{-5}	-9.92×10^{-5}	0	0	0	0	-7.97×10^{-4}	-3.25×10^{-3}
P_2	-3.77×10^{-3}	1.14×10^{-2}	-3.86×10^{-3}	-5.39×10^{-4}	-2.97×10^{-4}	-1.94×10^{-4}	-1.10×10^{-4}	-9.21×10^{-5}	-7.88×10^{-5}	-9.36×10^{-5}	0	0	0	0	-3.31×10^{-4}	-5.70×10^{-4}
P_3	-6.93×10^{-4}	-3.86×10^{-3}	1.13×10^{-2}	-3.19×10^{-3}	-7.62×10^{-4}	-3.62×10^{-4}	-1.72×10^{-4}	-1.28×10^{-4}	-9.88×10^{-5}	-1.07×10^{-4}	0	0	0	0	-2.05×10^{-4}	-2.72×10^{-4}
- -	- -	- -	- -	- -	- -	- -	- -	- -	- -	- -	- -	- -	- -	- -	- -	- -
P_{16}	-3.25×10^{-3}	-5.70×10^{-4}	-2.72×10^{-4}	-1.29×10^{-4}	-1.04×10^{-4}	-9.10×10^{-5}	-6.42×10^{-5}	-6.39×10^{-5}	-6.42×10^{-5}	-9.10×10^{-5}	0	0	0	0	-3.25×10^{-3}	9.81×10^{-3}

Table 9 Simulation image data for LBP in full – flow regime

Pixel No	Charge magnitude in (C) per sensor due to electric charge in pixel (i)															
	S_1	S_2	S_3	S_4	S_5	S_6	S_7	S_8	S_9	S_{10}	S_{11}	S_{12}	S_{13}	S_{14}	S_{15}	S_{16}
P_1	1.12×10^{-2}	-3.77×10^{-3}	-6.93×10^{-4}	-2.56×10^{-4}	-1.78×10^{-4}	-1.39×10^{-4}	-8.91×10^{-5}	-8.20×10^{-5}	-7.63×10^{-5}	-9.92×10^{-5}	-1.03×10^{-4}	-1.14×10^{-4}	-2.05×10^{-4}	-3.31×10^{-4}	-7.97×10^{-4}	-3.25×10^{-3}
P_2	-3.77×10^{-3}	1.14×10^{-2}	-3.86×10^{-3}	-5.39×10^{-4}	-2.97×10^{-4}	-1.94×10^{-4}	-1.10×10^{-4}	-9.21×10^{-5}	-7.88×10^{-5}	-9.36×10^{-5}	-8.81×10^{-5}	-8.89×10^{-5}	-1.41×10^{-4}	-1.89×10^{-4}	-3.31×10^{-4}	-5.70×10^{-4}
P_3	-6.93×10^{-4}	-3.86×10^{-3}	1.13×10^{-2}	-3.19×10^{-3}	-7.62×10^{-4}	-3.62×10^{-4}	-1.72×10^{-4}	-1.28×10^{-4}	-9.88×10^{-5}	-1.07×10^{-4}	-9.12×10^{-5}	-8.42×10^{-5}	-1.20×10^{-4}	-1.41×10^{-4}	-2.05×10^{-4}	-2.72×10^{-4}
- -	- -	- -	- -	- -	- -	- -	- -	- -	- -	- -	- -	- -	- -	- -	- -	- -
P_{16}	-3.25×10^{-3}	-5.70×10^{-4}	-2.72×10^{-4}	-1.29×10^{-4}	-1.04×10^{-4}	-9.10×10^{-5}	-6.42×10^{-5}	-6.39×10^{-5}	-6.42×10^{-5}	-9.10×10^{-5}	-1.04×10^{-4}	-1.29×10^{-4}	-2.71×10^{-4}	-5.70×10^{-4}	-3.25×10^{-3}	9.81×10^{-3}

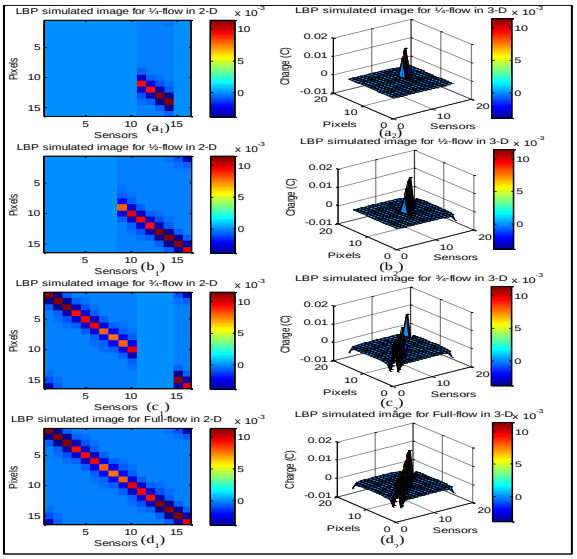

Figure 9 The simulation concentration profiles in LBP; (a1–c1) 2-D and (a2–d2) 3-D

3.2 The Experimental Set Up

In order to evaluate the image reconstruction using the developed sensitivity matrix; several experiments were carried out using the sixteen electrodynamics sensors installed around the gravity dropped conveying pipeline. The purpose of the experiment is to obtain data in the form of voltages from each of the 16 sensors. The obtained voltage data are in turn used the reconstruction of the concentration profile of the moving solid particles by the application of LBP method. Figure 10 shows the practical photographs of the experimental setup used for the data acquisition. The length between the rotary valve and the array of sensors was 1000 mm and the pipe internal diameter is 108 mm. In carrying out the experiment, the plastic bead particles are transported to the hopper through suction hose from the particles reservoir. The mechanical rotary valve of the hopper releases the particles which move under gravity and the electrostatic charges carried by the moving particles are captured by the 16 installed electrodynamic sensors. The particles are accelerated under gravity along the pipe vertical axis with an assumed acceleration due to gravity of 9.81 ms^{-2}.

Electrification occurs between the moving particles and the pipe wall during the conveying process. The process generates charges on the moving particles which in turn captured by electrodes of the electrodynamic sensors through induction. The induced charge is transduced into a voltage signal from the signal conditioning circuit attached to the sensor electrode. The voltage data from the sensors are used for the solid particles concentration profile across the pipeline cross-section of the flowing particles. The concentration profile reconstruction was done by the use of the LBP method. The experiments were carried out and the captured voltage data is shown in Table 10, whose bar chart is shown in Figure 11. The data captured by each of the 16 sensors, during the 4 flow regimes' experiments; were used to generate the real image data of Tables 11, 12, 13 and 14. The Figure 12 shows the concentration profiles of each of the 4 flow regimes in 2-D and 3-D.

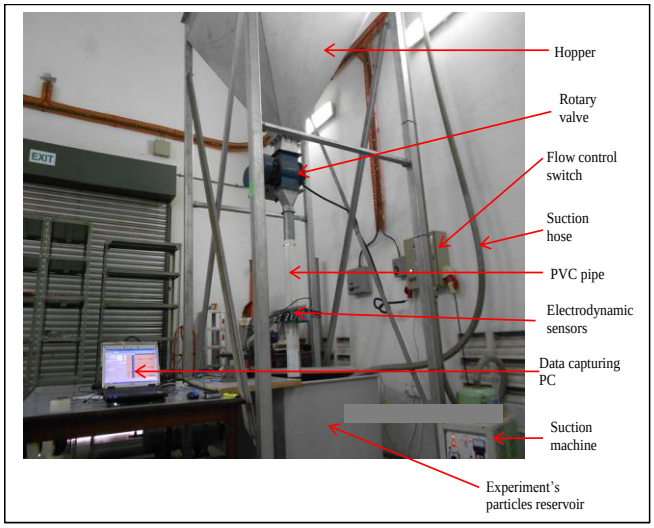

Figure 10 Experimental set up for the data capturing from the flowing solid particles

Table 10 The real induced average d.c voltages captured by the installed sensors during the 4 different flow regimes

Flow Regimes	Voltages (V_s) Captured by Sensors						
	S_1	S_2	S_3	S_4	S_5	--	S_{16}
¼-Flow	0.138	0.238	0.147	0.071	0.079	--	0.190
½-Flow	0.366	0.253	0.333	0.174	0.202	--	0.937
¾-Flow	0.939	1.036	1.000	0.903	1.179	--	0.824
Full-Flow	0.539	0.660	0.660	0.717	0.811	--	0.596

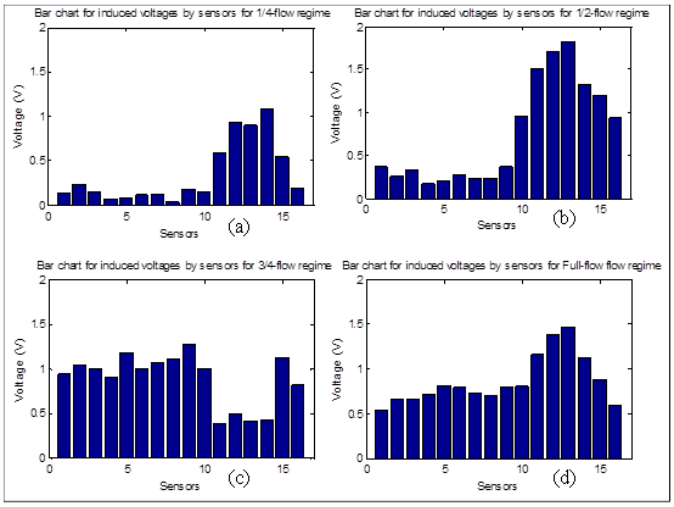

Figure 11 Bar Charts of the voltages captured by each of the sensors during the experiments (a) ¼-flow, (b) ½-flow, (c) ¾-flow and (d) Full-flow

Table 11 Extract from the real image data for LBP in ¼ -flow regime

Pixel No	Charge magnitude in (C) per sensor due to electric charge in pixel (i)						
	S_1	S_2	S_3	S_4	S_5	-	S_{16}
P_1	1.54×10^{-3}	-8.97×10^{-4}	-1.02×10^{-4}	-1.82×10^{-5}	-1.41×10^{-5}	-	-6.17×10^{-4}
P_2	-5.20×10^{-4}	2.72×10^{-3}	-5.67×10^{-4}	-3.83×10^{-5}	-2.34×10^{-5}	-	-1.08×10^{-4}
P_3	-9.56×10^{-5}	-9.18×10^{-4}	1.67×10^{-3}	-2.26×10^{-4}	-6.02×10^{-5}	-	-5.16×10^{-5}
- -	- -	- -	- -	- -	- -	- -	- -
P_{16}	-4.48×10^{-4}	-1.36×10^{-4}	-3.99×10^{-5}	-9.16×10^{-6}	-8.22×10^{-6}	-	1.86×10^{-3}

Table 12 Extract from the real image data for LBP in ½ -flow regime

Pixel No	Charge magnitude in (C) per sensor due to electric charge in pixel (i)						
	S_1	S_2	S_3	S_4	S_5	-	S_{16}
P_1	4.10×10^{-3}	-9.53×10^{-4}	-2.31×10^{-4}	-4.46×10^{-5}	-3.60×10^{-5}	-	-3.04×10^{-3}
P_2	-1.38×10^{-3}	2.89×10^{-3}	-1.28×10^{-3}	-9.38×10^{-5}	-5.99×10^{-5}	-	-5.34×10^{-4}
P_3	-2.54×10^{-4}	-9.76×10^{-4}	3.78×10^{-3}	-5.54×10^{-4}	-1.54×10^{-4}	-	-2.54×10^{-4}
- -	- -	- -	- -	- -	- -	- -	- -
P_{16}	-1.19×10^{-3}	-1.44×10^{-4}	-9.04×10^{-5}	-2.25×10^{-5}	-2.10×10^{-5}	-	9.20×10^{-3}

Table 13 Extract from the real image data for LBP in ¾ -flow regime

Pixel No	Charge magnitude in (C) per sensor due to electric charge in pixel (i)						
	S_1	S_2	S_3	S_4	S_5	-	S_{16}
P_1	1.05×10^{-2}	-3.90×10^{-3}	-6.93×10^{-4}	-2.32×10^{-4}	-2.10×10^{-4}	-	-2.67×10^{-3}
P_2	-3.54×10^{-3}	1.18×10^{-2}	-3.86×10^{-3}	$-4.87\times {}^{-4}$	-3.50×10^{-4}	-	-4.70×10^{-4}
P_3	-6.51×10^{-4}	-4.00×10^{-3}	1.13×10^{-2}	-2.88×10^{-3}	-8.99×10^{-4}	-	-2.24×10^{-4}
- -	- -	- -	- -	- -	- -	- -	- -
P_{16}	-3.05×10^{-3}	-5.90×10^{-4}	-2.72×10^{-4}	-1.17×10^{-4}	-1.23×10^{-4}	-	8.09×10^{-3}

Table 14 Extract from the real image data for LBP in Full – flow regime

Pixel No	Charge magnitude in (C) per sensor due to electric charge in pixel (i)						
	S_1	S_2	S_3	S_4	S_5	-	S_{16}
P_1	6.03×10^{-3}	-2.49×10^{-3}	-4.57×10^{-4}	-1.84×10^{-4}	-1.45×10^{-4}	-	-1.93×10^{-3}
P_2	-2.03×10^{-3}	7.54×10^{-3}	-2.55×10^{-3}	-3.87×10^{-4}	-2.40×10^{-4}	-	-3.40×10^{-4}
P_3	-3.74×10^{-4}	-2.55×10^{-3}	7.49×10^{-3}	-2.28×10^{-3}	-6.18×10^{-4}	-	-1.62×10^{-4}
- -	- -	- -	- -	- -	- -	- -	- -
P_{16}	-1.75×10^{-3}	-3.76×10^{-4}	-1.79×10^{-4}	-9.25×10^{-5}	-8.43×10^{-5}	-	5.85×10^{-3}

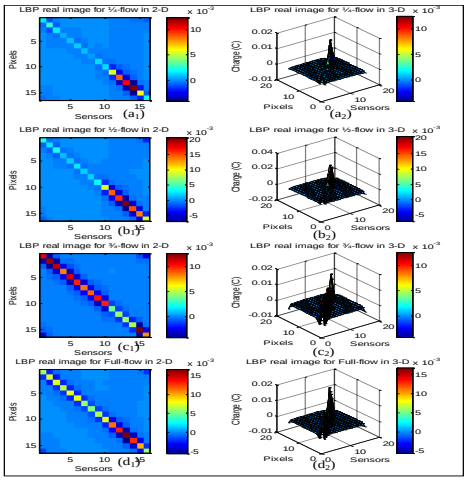

Figure 12 Real concentration profiles for each of the 4 flow regimes using LBP method; (a_1-d_1) is for 2-D while (a_2-d_2) are for 3-D

4.0 RESULTS AND DISCUSSION

In view of the paper title, there are two main results to be discussed, which are the sensitivity matrix and the reconstructed tomography images. In a system of linear equation that describes a system, the stability of the system is determined from the matrix system that defined the equation [18]. In a stable system, it is expected that a small changes in input produces a corresponding small changes in the output otherwise the system is unstable. Analysing an algorithm for stability is more complicated than determining the condition of an expression, even if the algorithm simply evaluates the expression. This is because an algorithm consists of many basic calculations and each one must be analysed and, due to round off error, we must consider the possibility of small errors being introduced in every computed value. This brings about the Condition numbers defined for any function as an expression of how sensitive those function is to small changes (or small errors) in its arguments [18]. It is imperative to note that the system of equation used in the generation of the sensitivity

matrix used in reconstruction of the concentration profile of the flowing solid particles of this research paper involved basic calculations from which small errors could be introduced. Nevertheless, the definition of the condition number for a system of equation defined in matrix form is the ratio of the largest value of the matrix S to the smallest value of the same matrix [19]. In the determination of the stability; if the condition number is finite and not more than 10^3; the system is stable. Which means that, the lower the condition number, the more stable is the system.

However in numerical analysis; the fundamental issues normally addressed in terms of the sensitivity of the solution to a specific form of problem is the accuracy of the values used in the problem. Therefore, accuracy is another important parameter in the numerical analysis of data used in a problem, which is an expression of lack of error and refers to, how closely multiple measurements of the same quantity cluster around the true value [20]. The assumption in practice is that, the mean of experimental data is the true value, where the mean of a set of measurement indicates the centre of the normal distribution [21]. This research developed mathematical formula used for the generation of sensitivity matrix; based on which, the data for the image reconstruction using LBP method were made. In the generation of the matrix, approximations were made that may result in errors.

However, the standard deviation has been associated with the error in each individual measurement which lies in the range of experimental values. The standard deviation is a measure of how widely a series of measurements is spread around the true (mean or average) value of a set of measurements. Therefore, the stability and accuracy of the data were analysed. For the stability analysis, the condition numbers of the two matrices; which are the main sensitivity matrix and the transposed sensitivity matrix, used for the image data were analysed and the results are 4.28 and 18.39 respectively. These show that, the system is well stable; because the condition numbers of the system of matrices used in the reconstruction of the tomography images are much less than 10^3.

For the accuracy of the image data, standard deviation error analysis was carried by the application of the following standard equation;

$$std_{error} = \sqrt{\frac{\sum_{i=1}^{n}(x(i)-\bar{x})^2}{n-1}} \quad (5)$$

Where

std_{error}= is the standard deviation

$\bar{X}$ = is the mean or average of the data

n= is the total number of measurements taken to obtain the dataset

$x(i)$= is the result of the i^{th} measurement.

The calculation using the Equation (5) is just an estimate from which an error of the estimation can be calculated by the use of the following relation;

$$\Delta std_{error} = \left[\frac{std_{error}}{\sqrt{2n-2}}\right] \quad (6)$$

The computation of the accuracy of the data is done by computing the estimated standard deviation of the image data and the error of estimation; by which statement on the accuracy of the system is made as shown in Table 15.

Table 15 Accuracy analysis for the simulation image data using the standard deviation error analysis

Imaging method	Flow regime data	Estimated standard deviation std_{error}	Error of estimation Δstd_{error}
Linear Back Projection (LBP)	¼-Flow	1.1×10^{-3}	4.9×10^{-5}
	½-Flow	1.8×10^{-3}	8.0×10^{-5}
	¾- Flow	8.0×10^{-4}	3.6×10^{-5}
	Full-Flow	9.1×10^{-4}	4.1×10^{-5}

The reconstructed image analysis is done by comparing the simulation and the real images. In this comparison, Figures 8 and 11 were compared to see if there is consistency in the simulation and captured data. The Figure 8, is an assumed captured voltage based on the baffling arrangement shown in Figure 7, while Figure 11 is the real data captured during the experimentation. It is clearly shown that, the sensors sense the charges on the flowing solid particles. This is because, the sensors that are exposed to the flowing particles in each of the flow regimes induces more charges than those that are not exposed.

However, consider Figure 7 (a) being the ¼-flow regime, the sensors 11, 12, 13 14 and 15 are directly exposed to the flowing solid particles and they are the sensors that induced higher charges than those that are blocked by the ¼-baffle, which induced very less charges, and is in agreement with the assumed induced charges in the Figure 8(a). In the reconstructed images shown in Figures 9 and 12, the distribution of the charges within the domain is in agreement with the sensors induced charges which is in the form of voltages shown in the bar charts of Figures 8 and 11 for the simulation and the real data respectively.

5.0 CONCLUSION

The basic requirement in process tomography image reconstruction is the development of the system equation that is used for the generation of the system's sensitivity matrix. In this research, the system equation was developed using the finite element techniques; where the mesh elements were structurally developed on the problem domain (pipeline cross-section). The same FEM was used to calculate the central Cartesian coordinates of each of the mesh elements. Based on these parameters, electrostatic laws were applied to develop the system equation that quantified the electrostatic charges carried by the flowing solid particles, on each of the mesh elements, as sensed by the 16 installed electrodynamic sensors. The equation was applied to generate the sensitivity matrix used for the image reconstruction.

To determine the stability of the system; condition number analysis was carried out on the system's sensitivity matrix and the accuracy of the data use for the image reconstruction were numerically analysed. To test the generated sensitivity matrix for the image reconstruction, LBP method was used on the experiments data, captured by the use of a standard gravity drop electric charge tomography test rig. In the experimentation, plastic beads particles flow through a test pipeline under gravity and the Keithley data acquisition instruments convert the charges on the moving solid particles that have been captured by the 16 installed electrodynamic sensors into voltage signal. It is the transduced voltage signal data that is used for the reconstruction of concentration profiles of the plastic solid particles for each of the 4 artificially created flow regimes. With

the theoretical and experimental results that are in conformity, the developed sensitivity matrix using the finite element method has been successfully implemented in image reconstruction in the electric charge tomography system. Since the system equation is in terms of the Cartesian coordinates of the mesh elements and the sensors; the proposed method of the sensitivity matrix generation can be applied in the other electric charge tomography instrumentation, such as; mass flow rate, particle sizing, velocity profile, particles identification etc.

Acknowledgement

The first author is grateful to the Nigeria Government through her Tertiary Education Trust (TET) Fund for sponsoring my PhD degree program with Universiti Teknologi Malaysia.

References

[1] I. T. Thuku, M. F. Rahmat, T. Tajdari, N. Abdul Wahab, and A. A. Yusuf. 2013. 2-D Finite-Element Modeling of Electrostatic Sensor for Tomography System. *Emerald: Sensor Review*. 33: 104–113.

[2] I. T. Thuku, M. F. Rahmat, and T. Tajdari. 2013. Electric Charge Tomography Imaging Using Finite-Element Method and Pro-rata Distribution. In *IEEE 8th International Conference on Industrial Electronics and Applications (ICIEA)*. Melbourne, Australia. 90–95.

[3] M. F. Rahmat. 1996. Instrumentation of Particle Conveying Using Electrical Charge tomography. PhD, Control Engineering, Sheffield Hallam, Sheffield.

[4] C. Soanes, S. Hawker, and J. Elliott. 2006. Oxford Dictionary of Current English. In *Oxford Dictionary of Current English Fourth Edition*. C. Soanes, S. Hawker, and J. Elliott, Eds., ed. USA: Oxford University Press. 1081.

[5] F. J. Dickin, B. S. Hoyle, A. Hunt, S. M. Huang, O. llyas, C. Lenn, *et al.* 1992. Tomographic Imaging of Industrial Process Equipment: Techniques and Applications. *IEE Proceedings-G*. 139: 72–82.

[6] T. Dyakowski, F. C. J. Laurent, and J. J. Artur. 2000. Applications of Electrical Tomography for Gas-Solids and Liquid-Solids Flows-a Review. *Powder Technology*. 112: 174–192.

[7] R. G. Green and R. Thorn. 1998. Sensor Systems for Lightly Loaded Pneumatic Conveyors. *Powder Technology ELSEVIER*. 95: 79–92.

[8] M. D. Isa. 2011. Least Square with Regularization Algorithm for Electric Charge Tomography System. PhD, Mechatronics and Control Engineering, Universiti Teknologi Malaysia, Johor Bahru.

[9] R. G. Green, M. F. Rahmat, K. Evans, A. Goude, and M. Henry. 1997. Concentration Profiles of Dry Powders in Gravity Conveyor Using an Electrodynamics Tomography System. *Measurement Science Technology*. 8: 192–197.

[10] M. F. Rahmat, M. D. Isa, A. R. Ruzairi, and A. R. H. Tengku. 2009. Electrodynamics Sensor for the Image Reconstruction Process in an Electrical Charge Tomography System. *Sensors*. 9: 10291–10308.

[11] I. T. Thuku, M. F. Rahmat, N. Abdul-Wahab, and T. Tajdari. 2014. Determination of Concentration Profile for Flowing Solid Particles in Pipeline Using Electric Charge Tomography System. *Mathematical Problems in Engineering, Hindawi Publishing Corporation*. 2014: 18.

[12] S. Jiaqing, J. Krabicka, and Y. Yan. 2010. Velocity Measurement of Pneumatically Conveyed Particles Using Intrusive Electrostatic Sensors. *Instrumentation and Measurement, IEEE Transactions on*. 59: 1477–1484.

[13] Z. Wenbiao, W. Chao, and W. Yulin. 2010. Parameter Selection in Cross-Correlation-Based Velocimetry Using Circular Electrostatic Sensors. *Instrumentation and Measurement, IEEE Transactions on*. 59: 1268–1275.

[14] J. Krabicka and Y. Yan. 2009. Finite-Element Modeling of Electrostatic Sensors for the Flow Measurement of Particles in Pneumatic Pipelines. *Instrumentation and Measurement, IEEE Transactions*. 58: 2730–2736.

[15] X. Y. Xiong, Z. T. Zhang, and W. Q. Yang. 2005. A stable Image Reconstruction Algorithm for ECT. *Journal Zhejiang University Science*. 6A: 1401–1404.

[16] W. Q. Yang and L. Peng. 2003. Review Article: Image Reconstruction Algorithms for Electrical Capacitance Tomography. *Measurement Science and Technology, Institute of Physics Publishing*. 14: 1–13.

[17] W. D. Yong and F. Dong. 2007. An Image Reconstruction Algorithm Based On Regularization Optimization for Process Tomography. In *SixthI nternational Conference on Machine Learning and Cybernetics*. Hong Kong. 1717–1722.

[18] G. Strang. 2009. *Introduction to Linear Algebra*. 4th ed. Massachusetts: Wellesley-Cambridge Press.

[19] G. Strang. 2007.*Computational Science and Engineering*. Second Printing. Wellesley MA, USA: Wellesley-Cambridge Press.

[20] ISO. 1994.Accuracy (Trueness and Precision) of Measurement Methods and Results–Part 1: General Principles and Definitions. ISO 5725-1.

[21] NIST/SEMATECH. e-Handbook of Statistical Methods, http://www.itl.nist.gov/div898/handbook/ ed, 2012.